# Demonstration of inverse scattering in optical coherence tomography

Tyler S. Ralston[a,b], Dan Marks[a,b], P. Scott Carney[a,b], and Stephen A. Boppart[a,b,c,*]

[a]Beckman Institute for Advanced Science and Technology
[b]Department of Electrical and Computer Engineering
[c]Department of Bioengineering, Internal Medicine
University of Illinois at Urbana-Champaign

## ABSTRACT

An object structure can be better resolved in optical coherence tomography by using inverse scattering theory, which takes into account the finite beam width and focusing. Specifically, we show experiments where scatterers are resolved outside of the confocal region such that resolution is uniform to the focused region. Numerical simulations demonstrate the effectiveness of this technique. When the algorithm is applied to experimentally-acquired OCT data, the transverse resolution outside of the confocal parameter is improved, extending the apparent confocal parameter range. The experimental results validate improvement for capabilities of OCT to perform high-resolution cross-sectional imaging.

Keywords: Optical coherence tomography, inverse scattering, Gaussian beam, transverse resolution, focusing.

## INTRODUCTION

Optical microscopy has long relied on the design of physical optical elements to produce images of samples. However, with the advent of scanning modalities such as confocal microscopy, near-field scanning optical microscopy and optical coherence tomography (OCT), image quality can determined as much by algorithm development as the quality of optical elements. Data synthesis and image formation algorithms have been crucial in other non-optical imaging modalities such as synthetic aperture radar (SAR) where improved algorithms have dramatically increased the performance of such systems. For example, the modeling of physical parameters has led to enhanced modes of strip-map and spotlight SAR imaging[1]. In these problems field quantities have been better defined thus providing a method for inverse of the data into an image.

Adaptive optics and axicon lenses are a selection of hardware for OCT which can help generate images with high transverse resolution over relatively large scanning depths in a specimen[2]. These optical techniques like dynamic focusing or focus tracking are useful for generating higher resolution cross-sectional imaging[3], where the tight focus is scanned in depth into the specimen[4]. Dynamic focusing techniques in a system design may require specific hardware modifications that can be difficult to control in real time. Some authors have designed algorithms that improve the axial resolution by compensating for the nonlinear dispersion between data in the temporal domain and the spatial domain[5]. Of these methods, some are used to correct for the limited bandwidth of the laser spectrum, while others correct for the dispersion induced by the optical system or the specimen. Modeling of the scattering processes has been limited to a one-dimensional quasi-monochromatic model[6]. These models do not take into account the relationship between data acquired at multiple transverse positions of the beam nor the finite transverse extent properties of the medium. Some authors have tried to correct for artifacts produced by sample positioning, refraction, and the scanning procedure[7]. In addition, others have detailed a theoretical model of OCT including a lens and heterodyning[8].

Our goal is to digitally reduce the distortion outside of the confocal region by solving the inverse problem based on the physics of the scattering process. We formulate a mathematical model to connect the experimentally acquired OCT signal with the three-dimensional object structure, taking into account the finite beam width and focusing. Therefore, by solving the inverse scattering problem, we can better determine the full structure of an imaged object from a data acquisition.

---

[*] For correspondence with Dr. Stephen A. Boppart email: boppart@uiuc.edu phone: (217) 244-7479

# OCT MODEL

In order to simplify the model for OCT data acquisition several assumptions are generally made about an OCT system. These assumptions do not take into account the shape of wavefronts produced by lens optics, the spectrum of the source, or even unbalanced dispersion in the media. Thus, many OCT images exhibit poor transverse resolution outside of the confocal region, which manifest as curved and blurred features obtained in these areas. The aspect of the inverse problem this work addresses is the resolution of scatterers outside of the confocal region in experimental OCT data.

An equation for the acquired OCT signal $S(\mathbf{r_0}, k) = A(k) \int_\Sigma d^2 r \int_V d^3 r' G(\mathbf{r'}, \mathbf{r}, k) g(\mathbf{r'} - \mathbf{r_0}, k) \eta(\mathbf{r'}) g(\mathbf{r} - \mathbf{r_0}, k)$ is presented in terms of our model, see Fig. 1. This equation represents the linear forward problem having the form of a type I Fredholm integral. The adjoint and the normal operators can be diagonalized by a coordinate transformation in the Fourier space such that a simplified least squares solution is formed. By solving the inverse problem, we are able to produce images with more sharply defined features. More importantly, we are able to distinguish closely adjacent scatterers, even those that produce interference in the raw OCT image. This is a crucial advantage of inverse scattering over simple deconvolution of a real valued point spread function.

The field at the output face of the fiber is given by $U_i(\mathbf{r})\big|_{z=0} = A(k)\phi(\mathbf{r})$. The field propagates to the plane $z = z_\ell$ where a thin lens is located. To the left of the $z = z_\ell$ plane, the field is given by the expression

$$U_i(\mathbf{r}) = A(k) \int d^2 r' P(\mathbf{r}, \mathbf{r'}) \phi(\mathbf{r'}), \tag{1.1}$$

where $P(\mathbf{r}, \mathbf{r'})$ is the free-space diffraction kernel. The lens is assumed to be a thin phase screen with transfer function given by $L(\mathbf{r})$, see Fig. 2. Thus, just to the right of the lens ($z = z_\ell$) the field is given by $U_i(\mathbf{r}) = A(k)L(\mathbf{r}) \int d^2 r' P(\mathbf{r}, \mathbf{r'}) \phi(\mathbf{r'})$. The field is focused into a Gaussian beam with beam waist in the $z = z_0$ plane. The field is given by the expression $U_i(\mathbf{r}) = A(k)g(\mathbf{r})$. Thus the normalized beam profile is also given by the expression

$$g(\mathbf{r}) = \int_{z'=z_\ell} d^2 r' L(\mathbf{r'}) \int_{z''=0} d^2 r'' P(\mathbf{r'}, \mathbf{r''}) \phi(\mathbf{r''}) P(\mathbf{r}, \mathbf{r'}). \tag{1.2}$$

The coupling of light back into the fiber is now derived in terms of the normalized waist plane field. Consider a field that propagates back toward the fiber and is given in some plane $\Sigma$ by $U_s(\mathbf{r})$ on the right side of the lens. The field may be propagated to the lens where it acquires the factor $L(\mathbf{r})$. The field incident on the fiber face $U_s(\mathbf{r})\big|_{z=0}$ will then be given by the expression,

$$U_s(\mathbf{r})\big|_{z=0} = \int_{z'=z_\ell} d^2 r' P(\mathbf{r}, \mathbf{r'}) L(\mathbf{r'}) \int_\Sigma d^2 r'' P(\mathbf{r'}, \mathbf{r''}) U_s(\mathbf{r''}). \tag{1.3}$$

The signal coupled into the single mode fiber is then given by the inner product of this field (Eq.(1.3)) and the fiber mode $\phi(\mathbf{r})$,

$$S = \int_{z=0} d^2 r \phi^*(\mathbf{r}) U_s(\mathbf{r}). \tag{1.4}$$

Equations (1.3) and (1.4) may be combined to yield

$$S = \int_{z=0} d^2 r \phi^*(\mathbf{r}) \int_{z'=z_\ell} d^2 r' P(\mathbf{r}, \mathbf{r'}) L(\mathbf{r'}) \int_\Sigma d^2 r'' P(\mathbf{r'}, \mathbf{r''}) U_s(\mathbf{r''}). \tag{1.5}$$

The field emerging from the fiber is assumed to be a diverging Gaussian beam with beam waist at $z$=0. Thus, $\phi^*(\mathbf{r}) = \phi(\mathbf{r})$. By comparing Eqs. (1.2) and (1.5) and noting $P(\mathbf{r''}, \mathbf{r'}) = P(\mathbf{r'}, \mathbf{r''})$, it may be seen that

$$S = \int_\Sigma d^2 r g(\mathbf{r}) U_s(\mathbf{r}). \tag{1.6}$$
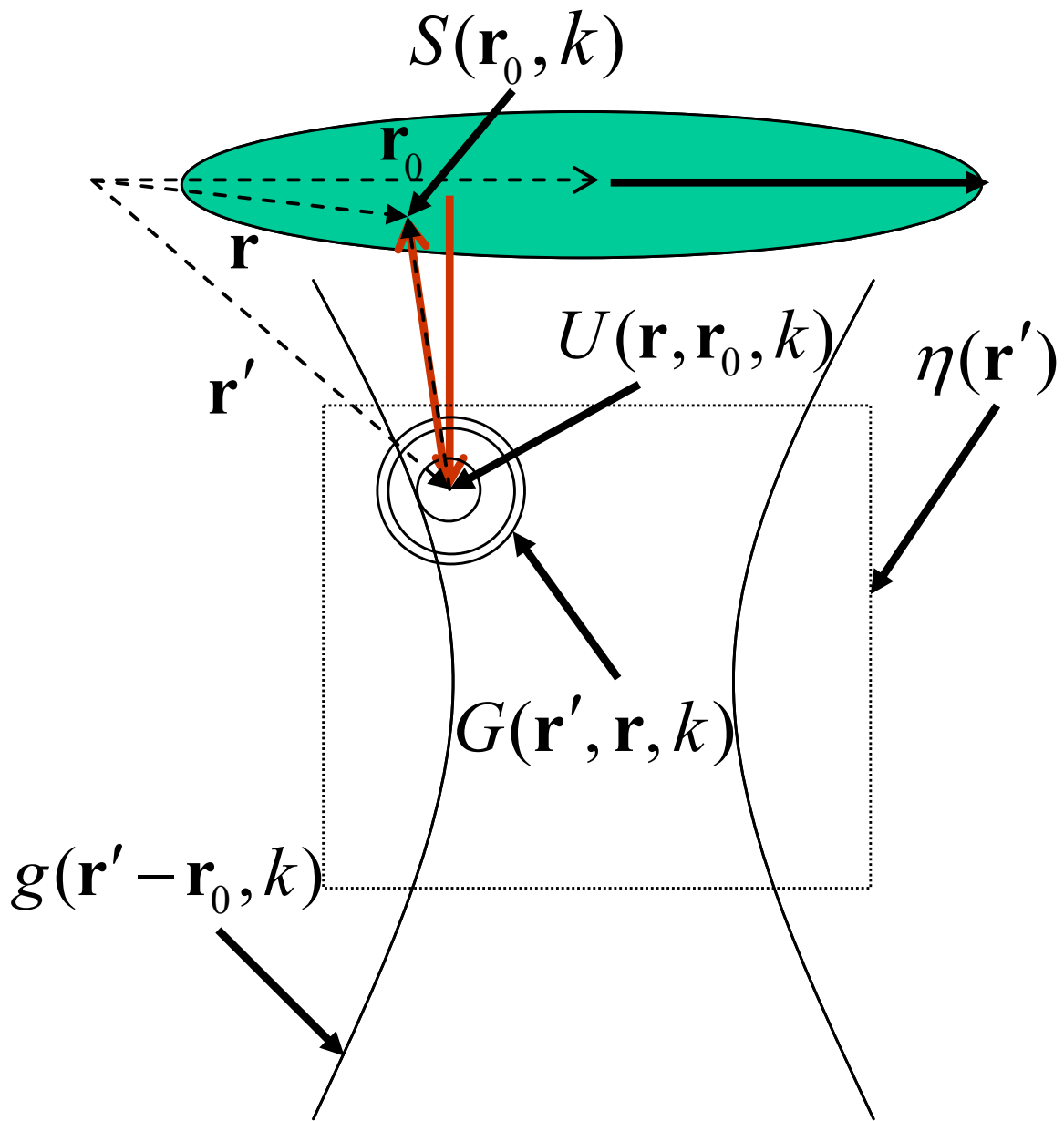
This is the expression for the signal used above.

Fig. 1. The diagram of scattering from a Gaussian beam, where $\mathbf{r_0}$ is the transverse position of the beam, $G(\mathbf{r'},\mathbf{r},k)$ is the radiated Green's Function, $g(\mathbf{r'}\text{-}\mathbf{r_0},k)$ is the translated incident field with a Gaussian beam profile, and $\eta(\mathbf{r'})$ is the susceptibility of the object. The vector $\mathbf{r'}$ describes a point in the object volume, and the vector $\mathbf{r}$ describes points on the boundary of the volume.

The signal may be written compactly as

$$\tilde{S}(\mathbf{Q},k) = i2\pi A(k)\int dz' H(\mathbf{Q},z',k)\tilde{\eta}(\mathbf{Q};z'),\qquad(1.7)$$

where $H(\mathbf{Q},z,k) = \int d^2 q \, \frac{1}{k_z(\mathbf{q})} e^{ik_z(\mathbf{q})(z-z_0)}\tilde{g}_0(\mathbf{q},k)e^{ik_z(\mathbf{Q}-\mathbf{q})(z-z_0)}\tilde{g}_0(\mathbf{Q}-\mathbf{q},k)$ .
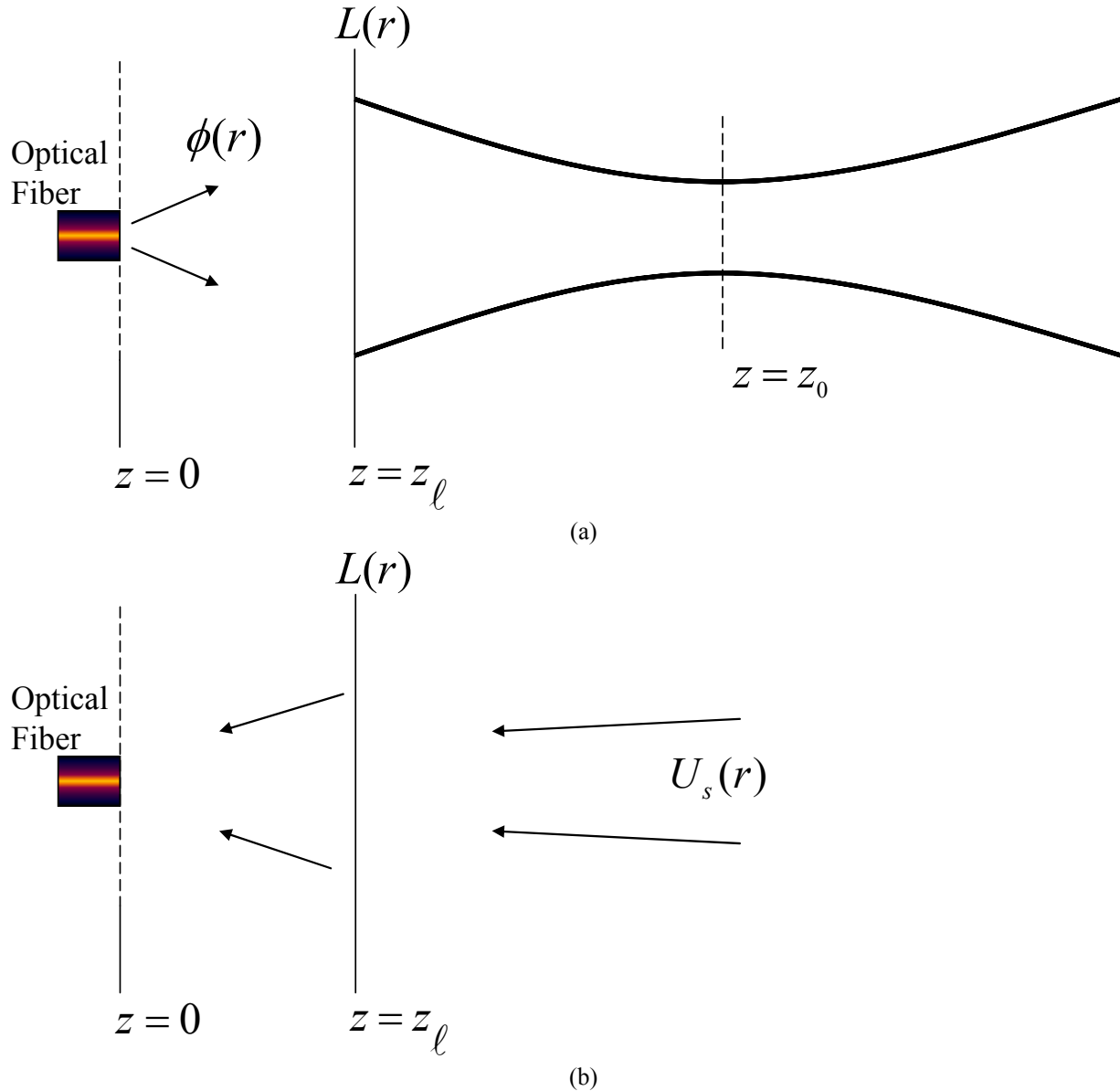
Fig. 2 Illustration of the coupling of light (a) out of, and (b) into the fiber.

The kernel $H$ takes the form

$$H(\mathbf{Q},z,k) = (\tilde{f} * \tilde{f})(\mathbf{Q},z,k) = \frac{1}{4\pi}\left(\frac{\alpha^2}{k^2} + i\frac{(z-z_0)}{k}\right)^{-1} e^{2i(z-z_0)k} e^{-\frac{Q^2}{2}\left(\frac{\alpha^2}{2k^2} + i\frac{(z-z_0)}{2k}\right)}. \tag{1.8}$$

Equation (1.7) may be seen to be a type I Fredholm integral equation and the kernel of the operator $K$ is apparent,

$$\tilde{S}(\mathbf{Q},k) = K\tilde{\eta}(\mathbf{Q}';z') = i2\pi A(k)\int dz' d^2Q' \; \delta^{(2)}(\mathbf{Q}-\mathbf{Q}')H(\mathbf{Q}',z',k)\tilde{\eta}(\mathbf{Q}';z'). \tag{1.9}$$

Substituting $\tilde{\eta}(\mathbf{Q}';z') = \dfrac{1}{2\pi}\int d\beta\, e^{i\beta z'}\tilde{\tilde{\eta}}(\mathbf{Q}';\beta)$, we obtain a representation for $K$

$$\tilde{S}(\mathbf{Q},k) = iA(k)\int d\beta\, d^2 Q'\, \delta^{(2)}(\mathbf{Q}-\mathbf{Q}')\, \tilde{H}(\mathbf{Q}',-\beta,k)\tilde{\tilde{\eta}}(\mathbf{Q}';\beta), \tag{1.10}$$

where, $\tilde{H}(\mathbf{Q},\beta,k) = \dfrac{k}{2}e^{-iz_0\beta}e^{\frac{\alpha^2}{k}(\beta-2k)}u\left(-\beta + 2k - \dfrac{Q^2}{4k}\right)$.     The Heaviside unit step function is denoted by

$$u(\beta) = \begin{cases} 1 & \beta > 0 \\ 0 & \beta \le 0 \end{cases}.$$

The kernel of the transform in Eq. (1.9),

$$H(\mathbf{Q},z,k) = \frac{1}{4\pi}\left(\frac{\alpha^2}{k^2} + i\frac{(z-z_0)}{k}\right)^{-1} e^{2i(z-z_0)k}e^{-\frac{Q^2}{2}\left(\frac{\alpha^2}{2k^2} + i\frac{(z-z_0)}{2k}\right)}, \tag{1.11}$$

must undergo a Fourier transform to arrive at Eq. (1.10).  Remember that our Fourier transform and inverse Fourier transform are defined by

$$\tilde{H}(\mathbf{Q},\beta,k) = \int dz\, e^{-i\beta z} H(\mathbf{Q},z,k), \tag{1.12}$$

and

$$H(\mathbf{Q},z,k) = \frac{1}{2\pi}\int d\beta\, e^{i\beta z}\, \tilde{H}(\mathbf{Q},\beta,k), \tag{1.13}$$

respectively.  Thus by substitution of Eq. (1.11) into Eq. (1.12), we attain

$$\tilde{H}(\mathbf{Q},\beta,k) = \int dz\, e^{-i\beta z}\frac{1}{4\pi}\left(\frac{\alpha^2}{k^2} + i\frac{(z-z_0)}{k}\right)^{-1} e^{2i(z-z_0)k}e^{-\frac{Q^2}{2}\left(\frac{\alpha^2}{2k^2} + i\frac{(z-z_0)}{2k}\right)}. \tag{1.14}$$

Next, we can pull out the constant $1/4\pi$ and rewrite $\left(\dfrac{\alpha^2}{k^2} + i\dfrac{(z-z_0)}{k}\right)^{-1}$ to fit a well-known Fourier transform form,

$$\tilde{H}(\mathbf{Q},\beta,k) = \frac{1}{4\pi}\int dz\, e^{-i\beta z} k\left(\frac{1}{\alpha^2/k + i(z-z_0)}\right)e^{2i(z-z_0)k}e^{-\frac{Q^2}{2}\left(\frac{\alpha^2}{2k^2} + i\frac{(z-z_0)}{2k}\right)}, \tag{1.15}$$

By introducing a phase shift term, $e^{i\beta z_0}$, inside and outside of the integral, we can complete the Fourier transform variable.

$$\tilde{H}(\mathbf{Q},\beta,k) = \frac{1}{4\pi}e^{-i\beta z_0}\int dz\, e^{-i\beta z}e^{i\beta z_0} k\left(\frac{1}{\alpha^2/k + i(z-z_0)}\right)e^{2i(z-z_0)k}e^{-\frac{Q^2}{2}\left(\frac{\alpha^2}{2k^2} + i\frac{(z-z_0)}{2k}\right)}, \tag{1.16}$$

Grouping all the $(z-z_0)$ terms to the right produces

$$\tilde{H}(\mathbf{Q},\beta,k) = \frac{1}{4\pi}e^{-i\beta z_0}\int dz\, ke^{-\frac{Q^2}{2}\left(\frac{\alpha^2}{2k^2}\right)}\left(\frac{1}{\alpha^2/k + i(z-z_0)}\right)e^{-i\beta(z-z_0)}e^{2i(z-z_0)k}e^{-\frac{Q^2}{2}\left(i\frac{(z-z_0)}{2k}\right)}. \tag{1.17}$$

Pulling all the integration, $dz$, constants out of the integral gives

$$\tilde{H}(\mathbf{Q},\beta,k) = \frac{1}{4\pi}e^{-i\beta z_0} ke^{-\frac{Q^2}{2}\left(\frac{\alpha^2}{2k^2}\right)}\int dz\, \left(\frac{1}{\alpha^2/k + i(z-z_0)}\right)e^{-i\beta(z-z_0)}e^{2i(z-z_0)k}e^{-\frac{Q^2}{2}\left(i\frac{(z-z_0)}{2k}\right)}. \tag{1.18}$$

Combining all the $(z-z_0)$ terms reduces $H$ to

$$\tilde{H}(\mathbf{Q}, \beta, k) = \frac{1}{4\pi} e^{-i\beta z_0} k e^{-\frac{Q^2}{2}\left(\frac{\alpha^2}{2k^2}\right)} \int dz \left(\frac{1}{\alpha^2/k + i(z - z_0)}\right) e^{-i(z-z_0)\left(\beta - 2k + \frac{Q^2}{4k}\right)}. \qquad (1.19)$$

Since $z_0$ is constant, $H$ is equivalently stated

$$\tilde{H}(\mathbf{Q}, \beta, k) = \frac{1}{4\pi} e^{-i\beta z_0} k e^{-\frac{Q^2}{2}\left(\frac{\alpha^2}{2k^2}\right)} \int d(z - z_0) \left(\frac{1}{\alpha^2/k + i(z - z_0)}\right) e^{-i(z-z_0)\left(\beta - 2k + \frac{Q^2}{4k}\right)}. \qquad (1.20)$$

The form of the Fourier transform of a unit step function times a decaying exponential, in this case for $\mathrm{Re}\{a\} > 0$, is known and is arrived at in the following way:

$$\int d\beta' \left[ e^{a\beta'} u(-\beta') \right] e^{iz'\beta'} = \int_{-\infty}^{0} d\beta' e^{a\beta'} e^{iz'\beta'} = \int_{-\infty}^{0} e^{(a+iz')\beta'} d\beta' = \frac{e^{\beta'(a+iz')}}{(a + iz')}\Bigg|_{-\infty}^{0} = \left(\frac{1}{a + iz'}\right). \qquad (1.21)$$

Therefore, one can see that

$$\frac{1}{2\pi} \int d\beta' \left[ e^{-a\beta'} u(\beta') \right] e^{-iz'\beta'} = \frac{1}{2\pi} \left(\frac{1}{a + iz}\right), \qquad (1.22)$$

and thus

$$\frac{1}{2\pi} \int d\beta' \left[ 2\pi e^{-a\beta'} u(\beta') \right] e^{-iz'\beta'} = \left(\frac{1}{a + iz}\right). \qquad (1.23)$$

This fits the form of our Fourier transform, hence

$$\tilde{H}(\mathbf{Q}, \beta, k) = \frac{1}{4\pi} e^{-i\beta z_0} k e^{-\frac{Q^2}{2}\left(\frac{\alpha^2}{2k^2}\right)} \int d(z - z_0) \left(\frac{1}{\alpha^2/k + i(z - z_0)}\right) e^{-i(z-z_0)\left(\beta - 2k + \frac{Q^2}{4k}\right)} \qquad (1.24)$$

can be evaluated to be

$$\tilde{H}(\mathbf{Q}, \beta, k) = \frac{1}{4\pi} e^{-i\beta z_0} k e^{-\frac{Q^2}{2}\left(\frac{\alpha^2}{2k^2}\right)} \left[ 2\pi e^{\frac{\alpha^2}{k}\left(\beta - 2k + \frac{Q^2}{4k}\right)} u\left(-\beta + 2k - \frac{Q^2}{4k}\right) \right]. \qquad (1.25)$$

The like terms can be grouped,

$$\tilde{H}(\mathbf{Q}, \beta, k) = \frac{1}{4\pi} e^{-i\beta z_0} k e^{-\frac{Q^2\alpha^2}{4k^2}} e^{\frac{Q^2\alpha^2}{4k^2}} \left[ 2\pi e^{\frac{\alpha^2}{k}(\beta - 2k)} u\left(-\beta + 2k - \frac{Q^2}{4k}\right) \right], \qquad (1.26)$$

and then reduced to

$$\tilde{H}(\mathbf{Q}, \beta, k) = \frac{k}{2} e^{-i\beta z_0} e^{\frac{\alpha^2}{k}(\beta - 2k)} u\left(-\beta + 2k - \frac{Q^2}{4k}\right). \qquad (1.27)$$

Remember that this solution is possible when considering a real, positive, bandlimited $k$.

## NUMERICAL SIMULATIONS

The goal of our numerical simulation is to demonstrate scattering and inverse scattering for a synthetic object. The forward OCT model simulates fringes from sub-resolution-sized point scatterers. Figure 3 displays simulated and reconstructed images of an imaging area of 1024 μm by 1024 μm, where the bandwidth is 340 nm, the focal length of the lens is 10 mm, the spot size is 4 μm, the confocal parameter is 30 μm, and the NA is 0.2. These parameters correspond to a NA and bandwidth larger than usually encountered in OCT systems in order to accentuate the distortion effects.
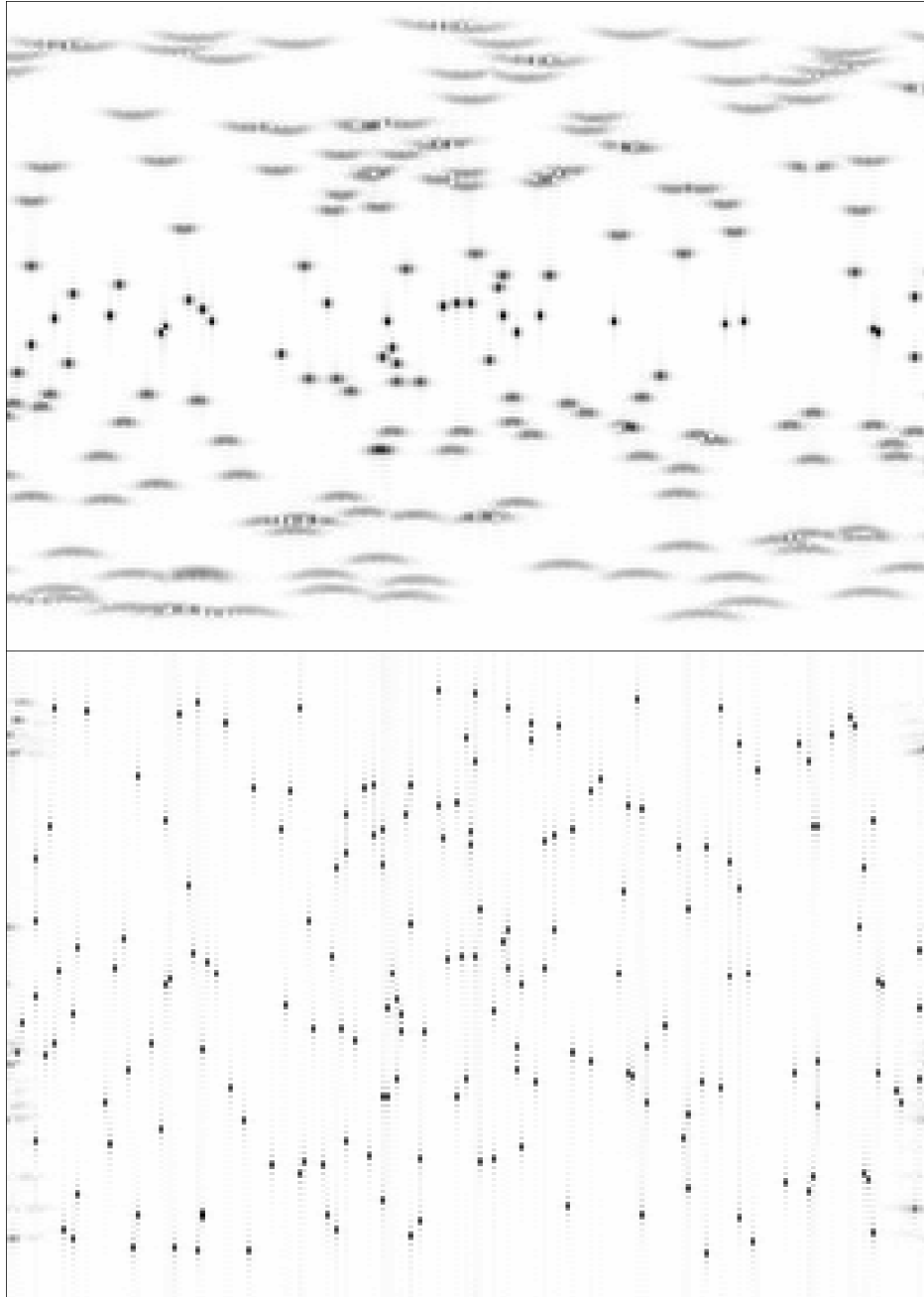
Fig. 3. Simulated OCT image, SNR = 35 dB (top), and Tikhonov regularized solution (bottom).

## EXPERIMENTAL DATA

A collection of 8 to 16 μm diameter scatterers were suspended in silicone and imaged with a spectral-domain OCT (SD-OCT) system. Figure 4 displays original and adjoint images of an imaging area of 500 (transverse) by 1000 μm (axial), where the bandwidth is 100 nm, the focal length of the lens is 20 mm, the spot size is 8 μm, and the confocal parameter is 125 μm. The transverse image resolution of point scatterers outside of the confocal region for the original experimental image data is not constant, but for the adjoint solution, the transverse resolution is relatively constant along the entire image with only amplitude variations.
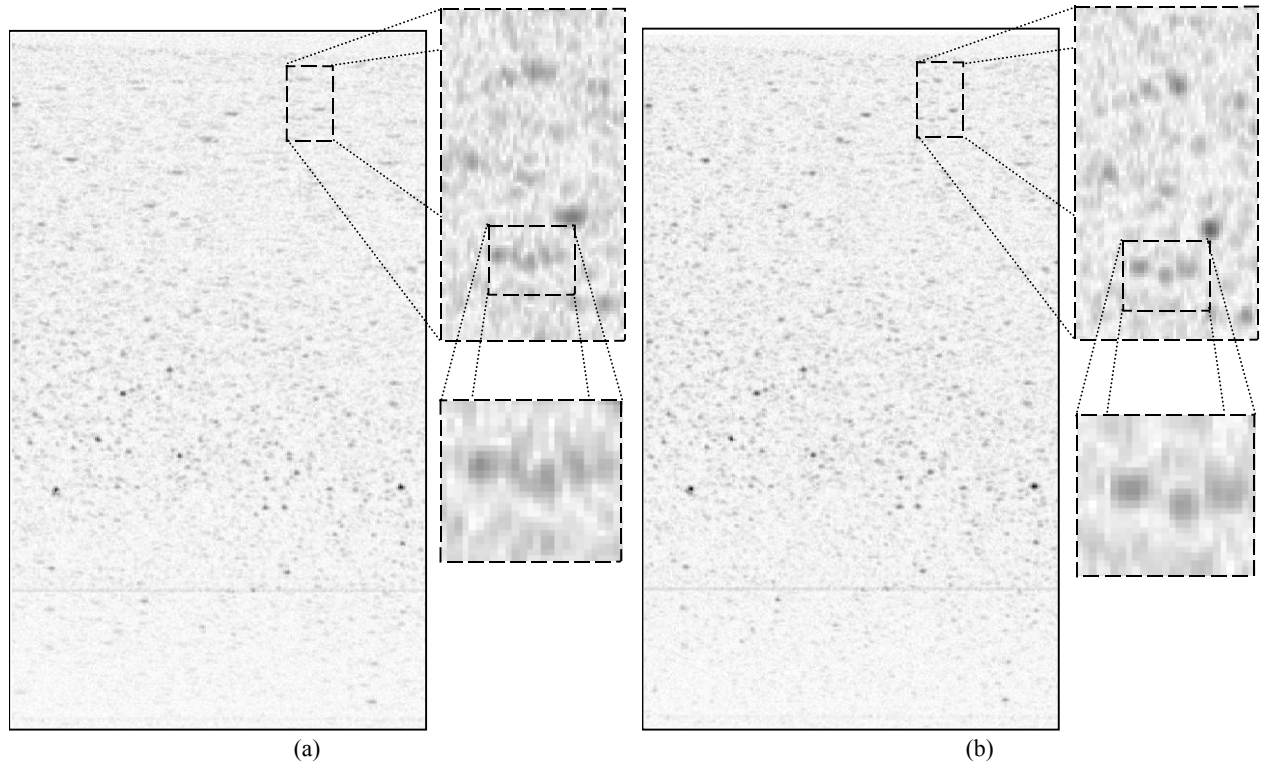
Fig. 4 Experimental SD-OCT images, (a) original (b) adjoint solution.

## CONCLUSIONS

A full model of OCT is presented for which the forward operator is formulated, thus giving rise to adjoint, normal, and inverse solutions. The results show that linear estimation of the susceptibility of an object from OCT data is possible when using an accurate model for the probe beam. Using regularization and the minimum norm solution, we can reconstruct underlying object structure with spatially invariant resolution in both simulated and experimental OCT image data sets, both of which contain regions of defocus. Two- and three-dimensional OCT data can be used for resolving objects and recovering high-resolution details outside of the confocal region with minimal loss of resolution. The model presented accounts for the effects of the source spectrum and the finite beam width, as well as dispersion, diffraction, and defocus effects.

## REFERENCES

1.  Cooper, P. S., Wons, A. F. & Gaskell, A. P. High resolution synthetic aperture radar using a multiple sub-band technique. *IEE Radar*, 263-267 (1997).
2.  Ding, Z., Ren, H., Zhao, Y., Nelson, J. S. & Chen, Z. High-resolution optical coherence tomography over a large depth range with an axicon lens. *Optics Letters* **27**, 243-245 (2002).
3.  Schmitt, J. M. Optical Coherence Tomography (OCT): A Review. *IEEE Journal of Selected Topics in Quantum Electronics* **5**, 1205-1215 (1999).
4.  Cobb, M. J., Liu, X. & Li, X. Continuous focus tracking for real-time optical coherence tomography. *Optics Letters* **30**, 1680-1682 (2005).
5.  Kulkarni, M. D., Thomas, C. W. & Izatt, J. A. Image enhancement in optical coherence tomography using deconvolution. *Electronics Letters* **33**, 1365-1367 (1997).
6.  Bruno, O. & Chaubell, J. One-dimensional inverse scattering problem for optical coherence tomography. *Institute of Physics Publishing, Inverse problems*, 499-524 (2005).

7.  Podoleanu, A., Charalambous, I., Plesea, L., Dogariu, A. & Rosen, R. Correction of distortions in optical coherence tomography imaging of the eye. *Institute of Physics Publishing, Physics in Medicine and Biology*, 1277-1294 (2004).
8.  Feng, Y. & Wang, R. K. Theoretical model of optical coherence tomography for system optimization and characterization. *Journal of the Optical Society of America* **20**, 1792-1803 (2003).